PCCP

Accepted Manuscript

This is an *Accepted Manuscript*, which has been through the Royal Society of Chemistry peer review process and has been accepted for publication.

Accepted Manuscripts are published online shortly after acceptance, before technical editing, formatting and proof reading. Using this free service, authors can make their results available to the community, in citable form, before we publish the edited article. We will replace this *Accepted Manuscript* with the edited and formatted *Advance Article* as soon as it is available.

You can find more information about *Accepted Manuscripts* in the **Information for Authors**.

Please note that technical editing may introduce minor changes to the text and/or graphics, which may alter content. The journal's standard **Terms & Conditions** and the **Ethical guidelines** still apply. In no event shall the Royal Society of Chemistry be held responsible for any errors or omissions in this *Accepted Manuscript* or any consequences arising from the use of any information it contains.

ARTICLE TYPE

Photoinduced Molecular Dissociation and Photoinduced Recombination Mediated by Superfluid Helium Nanodroplets

Andreas Kautsch, Markus Koch,[*] **and Wolfgang E. Ernst**[*]

We have investigated photoinduced chemical reaction dynamics of cold, isolated Cr_2 molecules in helium nanodroplets (He_N), exploiting the quantum state specific spatial separation of solvated and surface locations on the droplet. The molecules are excited to achieve dissociation to a ground state (a^7S_3) and a metastable state (a^5S_2) atom. State specific spatial separation, in combination with efficient translational cooling to avoid ejection, causes the ground state atom to be solvated inside the droplet while the metastable atom migrates to the surface. A barrier between the two reactants formed by the He_N prevents recombination. We apply a resonance-enhanced multiphoton ionization scheme including the $y^5P^\circ_{1,2,3} \leftarrow a^5S_2$ transition of the surface atom as well as a two-laser scheme including the $y^7P^\circ_{2,3,4} \leftarrow a^7S_3$ transition of the solvated atom in order to verify the locations and separation of the dissociation products. Furthermore, ionization of the a^5S_2 surface atom triggers solvation followed by geminate recombination with the a^7S_3 atom, which is verified by the detection of Cr_2^+ molecular ions. For small Cr clusters, our results indicate that they may be composed of chromium dimers that exhibit the same dissociation behavior.

Keywords: cold molecules, isolation, predissociation, resonant multiphoton ionization, chromium clusters

1 Introduction

Helium nanodroplets (He_N) represent a well-established matrix for the spectroscopic investigation of isolated, cold (0.4 K) atoms, molecules, and clusters[1] and offer a unique method for cold chemistry on a single molecule level. The spatial separation of surface located and solvated dopants in He_N provides a promising approach to control and monitor chemical reactions, especially if the location is state specific and can thus be changed by photoexcitation. In this article we demonstrate a complete cycle of photoinduced molecular dissociation, spatial separation of the fragments to a fully solvated and a stable, surface bound state and finally, photoinduced geminate recombination of the fragments.

Increasing interest in exploring chemical reactions in He_N originates from the ability to stabilize and investigate radical reaction intermediates[2–7] or confine dissociation fragments to the volume of the droplet[8,9]. High cooling rates permit efficient relaxation of excited molecules[1,8], the formation and stabilization of metastable clusters[10,11], or aggregation of weak Van der Waals bound complexes (see, e.g., Ref.[12]). Shallow energy barriers along reaction pathways can lead to trapping in local reactive potential-energy surface minima[4] which

can be overcome by photo-activation to trigger chemical reactions[13,14]. The location of a dopant is dictated by the interaction with helium (the pair potential) and can be estimated by the dimensionless Ancilotto parameter[15]. While the majority of atoms and molecules in their ground state are located inside the droplet, an electronic transition from the ground state to an excited state can initiate migration from inside to the droplet surface. This has been observed, for example, for Ag[16–18], Cu[19,20], Cr[21–23], CF_3[24,25], and NO[26]. Usually, surface migration is followed by desorption from the droplet, only for NO* there was indication that the excited molecule remains in a surface-bound state[26]. For droplets doped with both surface located and solvated species the helium matrix can form a barrier that prevents molecule formation or clustering, even in the presence of long range Van der Waals interaction[27]. On the other side, Van der Waals forces between solvated noble gas atoms and surface-located alkaline earth metal atoms can be exploited to overcome the separating character of He_N[28,29]. Transition from a surface location to solvation was achieved for the HCN-Sr complex (and vice versa for HCN-Ca) by vibrational excitation[30], and in general, surface-located species migrate inside the droplet upon ionization[31–34].

Here we demonstrate that photoexcitation of solvated Cr_2 molecules results in dissociation to one atom in a solvated state (a^7S_3) and a second atom in a surface bound state (a^5S_2). Both fragments are sufficiently cooled to prevent ejection from

Graz University of Technology, Institute of Experimental Physics, NAWI Graz, Petersgasse 16, A-8010 Graz, Austria, EU
[*] To whom correspondence should be addressed: markus.koch@tugraz.at, wolfgang.ernst@tugraz.at

the droplet. A resonant three photon ionization scheme is applied to the surface atom to verify its location and, at the same time, trigger solvation and recombination with its original partner. The stable interior location of the other fragment is proven with a two laser experiment, where both lasers are scanned individually.

2 Experimental

Chromium clusters (Cr_2 - Cr_4) are formed inside helium nanodroplets by the pickup of single Cr atoms. The setup follows a Helium Nanodroplet Isolation (HENDI) apparatus, described in detail in Ref.[35]. In brief, He_N are formed by the supersonic expansion of high purity ^4He gas through a cooled nozzle (diameter d = 5 μm, stagnation pressure p_0 = 50 bar). Droplet sizes follow a log-normal distribution with a distribution maximum of $\hat{N}$ = 6 300 He atoms (mean droplet size $\bar{N}$ = 16 000) for a nozzle temperature of 14 K. The collimated He_N beam is crossed at right angles by an effusive beam of Cr atoms from an electron bombardment Cr oven[36] beneath the He_N beam. This setup ensures that no free atoms reach the detection region. To characterize the pick-up conditions, the number of $Cr_{1,2,...}^+$ ions formed by electron bombardment ionization is monitored as function of the oven heating power. A quadrupole mass spectrometer (QMS, Balzers QMG 422) is attached at the end of the measurement chamber to facilitate mass selective ion detection. This allows an assignment of the photoion signal to a specific Cr_n cluster size, by comparing the photoion yield to the electron bombardment $Cr_{1,2,...}^+$ yield as a function of heating power.

Excitation spectra of the Cr_n-He_N (n = 2-4) complexes are recorded with resonance-enhanced multiphoton ionization (REMPI) spectroscopy[21]. Laser pulses are obtained from excimer (XeCl, Radiant Dyes RD-EXC-200, 308 nm, ~20 ns pulse duration) pumped dye lasers. For one-color REMPI, a pulsed dye laser beam (Lamda Physik, FL3002, dyes: Coumarin 2, Coumarin 102) intersects the doped He_N beam at right angles in the extraction region of the QMS. The mass window of the QMS is set to integrate the signal of the Cr_n^+ isotopes and Cr_n^+-He around the central cluster mass to increase the signal. To further increase the signal quality, two-color REMPI is used in addition[23]. Therefore, a fraction of the 308 nm pump laser light is overlapped with the dye laser.

A pump-probe scheme is applied to observe the formation of ground state atoms after dissociating Cr_2. Two dye laser beams (Radiant Dyes, DL-midi, dye: Coumarin 2; Lamda Physik, FL3002, dye: RDC360 neu) intersect the doped He_N beam, where the first one dissociates the molecules, while the second ionizes the produced ground state Cr atoms state selectively with a known REMPI scheme[21]. In addition to the signal from dissociated Cr_2, single Cr atom doped He_N cause a background signal, which is subtracted by a difference de-

tection scheme (dissociation laser on minus off). The fluence of the dissociation laser is kept low in order to prevent ionization of the dissociation products (in contrast to the experiment described above).

In Fig. 1 the Cr_2 potential energy curves[37,38] and Cr atom energy levels[39] that are of relevance for the presented experiments are shown, together with an excitation-ionization scheme indicated with arrows. The first step in this scheme is excitation of ground state Cr_2 ($4\sigma^2 3d\sigma^2 3d\pi^4 3d\delta^4$[40]) inside He_N via the $A^1\Sigma_u^+ \leftarrow X^1\Sigma_g^+$ transition. The excited $A^1\Sigma_u^+$ state correlates to one ground state (a^7S_3, $3d^54s$) and one excited ($z^7P°$, $3d^54p$) Cr atom, and, as will be shown below, dissociates via internal conversion to form one a^7S_3 and one a^5S_2 ($3d^54s$) atom.

3 Results

One-color REMPI excitation spectra of Cr_2 via the $A^1\Sigma_u^+ \leftarrow X^1\Sigma_g^+$ transition for Cr^+ and Cr_2^+ detection are shown in Fig. 2 (a). The broad band, stretching from 21500 to 22750 cm^{-1}, is attributed to the Cr_2 $A^1\Sigma_u^+ \leftarrow X^1\Sigma_g^+$ transition and the three pronounced peaks can be assigned to Cr atom $y^5P°_{1,2,3} \leftarrow a^5S_2$ transitions (indicated by triangles[39]). Because the $A^1\Sigma_u^+ \leftarrow X^1\Sigma_g^+$ molecular band overlaps with the atomic transition energies, these peaks indicate the photoinduced dissociation with one of the fragments being in the a^5S_2 state, as will be discussed in detail below. The whole excitation-ionization process from a^5S_2 is indicated with solid, upwards pointing arrows in Fig. 1. Cr_2 is excited to a predissociating state that leads to the formation of a ground state a^7S_3 and a metastable state a^5S_2 atom[41]. The latter is excited via the $y^5P°_{1,2,3} \leftarrow a^5S_2$ transition and ionized with either two (one-color REMPI) or one (two-color REMPI) photon. This ionization path selectively addresses a^5S_2 metastable Cr atoms and will be called **a^5S REMPI** from now on. For further insight into the dynamics after dissociation, we present detailed scans across the $y^5P°_3 \leftarrow a^5S_2$ transition for the detection of Cr^+ to Cr_4^+ in Fig. 3. Although one-color and two-color REMPI give equal results, the latter provides a better signal to noise ratio and was thus chosen. One 308 nm photon is used for ionization of excited $y^5P°_3$ state atoms instead of two dye laser photons (c.f. Fig. 1). The spectral signature is similar for detection of $Cr_{1,2,3,4}^+$, where the appearance of $Cr_{3,4}^+$ is connected to larger Cr_n (n = 3, 4, ...) clusters, as will be discussed in section 4.

While the production of the metastable a^5S_2 atom as one of the dissociation products is verified with a^5S REMPI (see Fig. 2 (a) and Fig. 3), the verification of the other dissociation product - the a^7S_3 ground state atom - requires a second laser. It ionizes the a^7S_3 atom with a well known Cr one-color REMPI scheme[21] that includes the $y^7P°_{2,3,4} \leftarrow a^7S_3$ ground
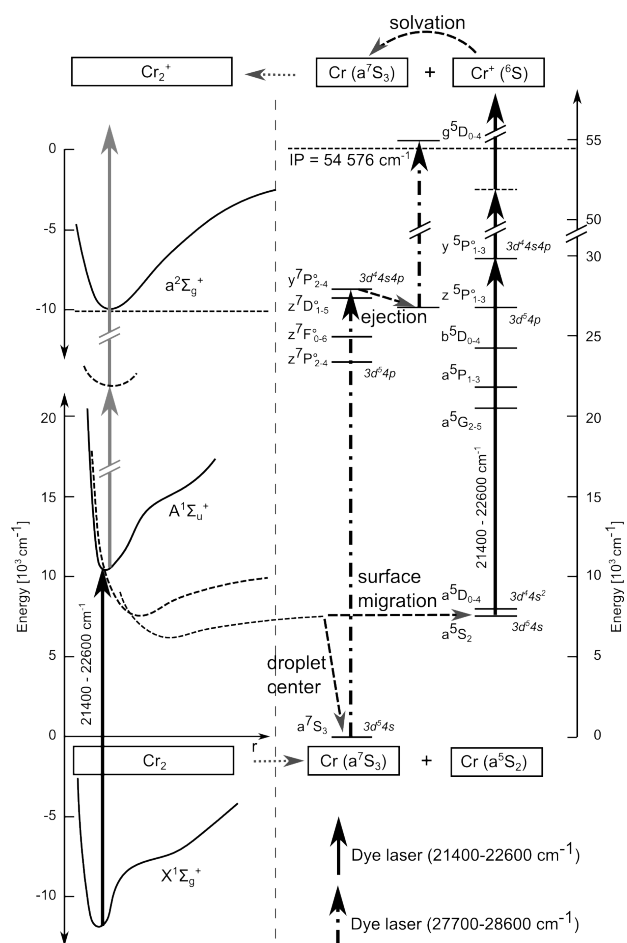
Fig. 1 Cr_2 and Cr_2^+ potential energy curves[37,38] (left) and Cr atom energy levels[39] (right). A one-color ionization scheme is indicated by a combination of solid arrows (laser excitation) and dashed arrows (relaxation). Upon Cr_2 excitation to the $A^1\Sigma_u^+$ state inside He_N, the molecule undergoes relaxation to predissociating states resulting in a^7S_3 Cr and a^5S_2 Cr atom states. While the first remains solvated inside the droplet, the latter migrates to the surface where it is ionized by a resonant three photon scheme. This triggers solvation and recombination to Cr_2^+ (top of the figure). The ionization path to probe the ground state atom with a second dye laser is indicated by dash-dotted arrows[21]. A suggested ionization path that does not include Cr_2 dissociation is indicated by gray arrows.
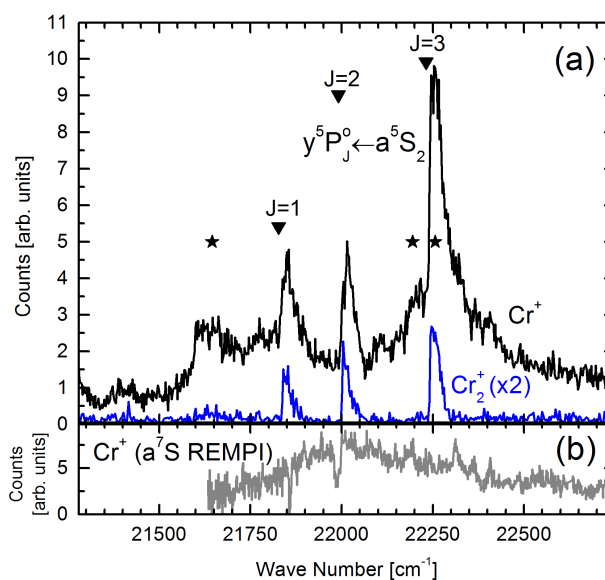
Fig. 2 (Color online) (a) One-color REMPI spectra in the range of the Cr_2 $A^1\Sigma_u^+ \leftarrow X^1\Sigma_g^+$ transition. Photoions are detected at the mass of Cr^+ (black line) and Cr_2^+ (blue line, multiplied by 2). The bare Cr atom $y^5P_{1,2,3}^\circ \leftarrow a^5S_2$ transition energies are indicated with triangles[39]. Asterisks mark the wavelengths at which the photoion yield is compared to the $Cr_{1,2,...}^+$ ion yield obtained with electron impact ionization in dependence on the pick-up oven temperature. (b) Excitation spectrum in the range of the Cr_2 $A^1\Sigma_u^+ \leftarrow X^1\Sigma_g^+$ transition, recorded with a pump-probe laser scheme. The dissociating laser is scanned across the Cr_2 band, while the second laser ionizes the produced ground state atoms with a^7S REMPI (includes the $y^7P_{2,3,4}^\circ \leftarrow a^7S_3$ transition). Narrow dips and peaks are artifacts due to experimental instabilities.
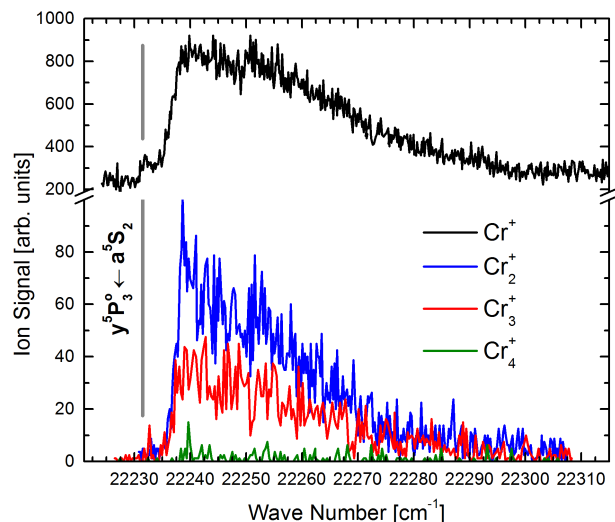
Fig. 3 (Color online) High resolution REMPI scan of the $y^5P_3^\circ \leftarrow a^5S_2$ transition within the Cr_2 $A^1\Sigma_u^+ \leftarrow X^1\Sigma_g^+$ band (Fig. 2) for detection of $Cr_{1,2,3,4}^+$ ions (two-color ionization scheme with the XeCl laser at 308 nm as second wavelength). The bare Cr atom $y^5P_3^\circ \leftarrow a^5S_2$ transition energy is indicated with a vertical line[39].
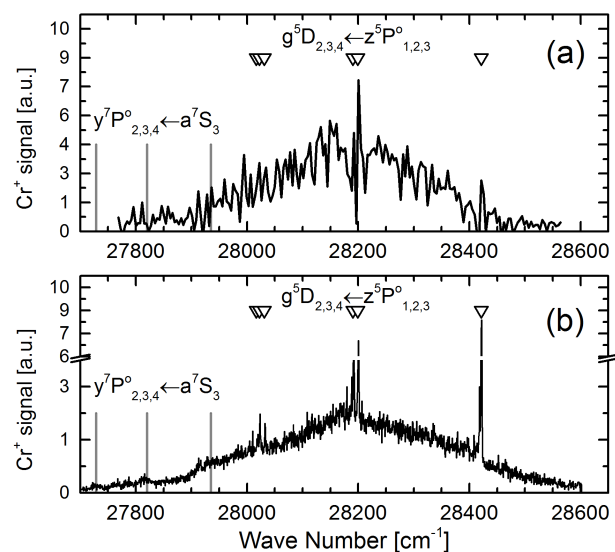
Fig. 4 a^7S_3 REMPI spectra of ground state Cr atoms in He_N. (a) Spectrum recorded in a two laser experiment, where the Cr_2 dissociation laser is fixed ($\bar{\nu} = 21978$ cm^{-1}) and the second laser (a^7S_3 REMPI) is scanned. A difference scheme (dissociation laser on minus off) was applied. (b) a^7S_3 REMPI spectrum for single Cr-atom doped He_N[21]. The bare Cr atom ground state transitions $y^7P_{2,3,4}^\circ \leftarrow a^7S_3$ are indicated as vertical lines and transitions to AI states with triangles.

state transition (Fig. 1, dash-dotted arrows) and is called **a^7S REMPI** from now on. The two-laser scheme opens the possibility to scan both laser wavelengths individually. First, the dissociation process is studied (Fig. 2 (b)) by scanning the dissociation laser across the Cr_2 excitation band and photoionizing the produced ground state atoms with a^7S REMPI ($\bar{\nu} = 28204$ cm^{-1}). Note that a certain fraction of the He_N are originally doped with single a^7S_3 Cr atoms according to the pick-up statistics. Hence, for all two dye laser experiments a differential measurement is applied to subtract these atoms from the Cr_2 dissociation signal.

To gain information about the location of the a^7S_3 Cr atom, the dissociating laser wavelength is kept constant at $\bar{\nu} = 21978$ cm^{-1} and the a^7S laser is scanned across the atomic $y^7P_{2,3,4}^\circ \leftarrow a^7S_3$ ground state transition. It was shown for single Cr atoms solvated inside He_N, that the $y^7P_{2,3,4}^\circ \leftarrow a^7S_3$ ground state transition is shifted and broadened by about 400 to 600 cm^{-1} due to the Pauli repulsion of the surrounding Helium[21–23]. As indicated in Fig. 1, after excitation to $y^7P_{2,3,4}^\circ$ the atoms are ejected from the droplet while relaxing to energetically lower states (e.g., $z^5P_{1,2,3}^\circ$)[21–23]. This mechanism enables a highly efficient ionization of bare atoms with one further laser photon, also through Cr autoionizing states that lie close to the ionization potential (g^5D, e^3D). The spectrum with the fixed dissociating laser and the a^7S REMPI laser scanning across the ground state transition is shown in Fig. 4 (a). Due to a difference scheme, the spectrum can be allocated to Cr atoms from dissociated Cr_2, detected at the Cr^+ mass. For comparison, the spectrum obtained with a^7S REMPI of single Cr atoms in He_N (not via dissociation of Cr_2) is plotted in Fig. 4 (b) (from Ref.[21]). In both spectra, the broad structure is attributed to the in-droplet $y^7P_{2,3,4}^\circ \leftarrow a^7S_3$ ground state excitation, which is very similar regarding shape and position. The narrow peaks (indicated with triangles) are allocated to the bare atom $g^5D_{2,3,4} \leftarrow z^5P_{1,2,3}^\circ$ autoionizing transitions. The experimental conditions, i.e. droplet size, for the spectrum in Fig. 4 (a) are optimized for Cr_2 formation resulting in a lower signal to noise ratio and reduced AI peaks[23]. A very similar spectrum to Fig. 4 (a) was obtained when delaying the a^7S REMPI probe laser pulse by 20 ns with respect to the dissociating pump laser pulse, so that there is no temporal overlap between the pulses.

4 Discussion

4.1 Predissociation

Photoinduced dissociation in He_N has been observed for various species[13,25,28,42]. Predissociation of Cr_2 upon excitation to $A^1\Sigma_u^+$ has been observed in gas phase[37,41,43] and in matrix[40]. It was concluded, that the $A^1\Sigma_u^+$ state is crossed by at least one perturbing state and one predissociating state, where

possible assignments were discussed by Andersson[37]. Riley et al.[41] propose the nonradiative transition from the $A^1\Sigma_u^+$ to another bound state. The latter is rapidly dissociated by a state correlating to the separate atom limit states Cr (a^7S_3) and Cr (a^5S_2, a^5D)[41]. From the observation of the $y^5P_{1,2,3}^\circ \leftarrow a^5S_2$ and $y^7P_{2,3,4}^\circ \leftarrow a^7S_3$ atomic transitions, we clearly identify the population of the a^5S_2 and a^7S_3 atom states and assign the following dissociative process:

$$Cr_2(X^1\Sigma_g^+) \xrightarrow{h\nu} Cr_2(A^1\Sigma_u^+) \longrightarrow Cr(a^7S_3) + Cr(a^5S_2) \quad (1)$$
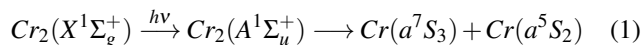
4.2 Separation to a surface located a^5S_2 and a solvated a^7S_3 atom

The fate after dissociation is dictated by the interaction of the Cr atoms in the respective state (a^7S_3, a^5S_2) with He atoms[44,45]. In principle, the atoms can remain solvated inside the He_N, stay bound on the surface, or detach from the He_N with a certain probability to take a few He atoms along. Since the droplet acts as a heat bath, kinetic energy can be dissipated to prevent ejection[8,9]. An excess energy of about 0.4 eV (3200 cm^{-1}), given by the difference of excitation energy and the dissociation limit (c.f. Fig. 1), can be compensated by the evaporation of 640 He atoms. So the location of the dopants after dissociation is governed by the electronic states of the atoms. Experimentally, the location of the two fragments is obtained from the lineshapes of the a^7S REMPI (via $y^7P_{2,3,4}^\circ \leftarrow a^7S_3$) and the a^5S REMPI (via $y^5P_{1,2,3}^\circ \leftarrow a^5S_2$) spectra. As observed for single Cr atoms in earlier experiments[21–23] and as predicted by theoretical studies[44,45], the ground state (a^7S_3) atom remains solvated inside the droplet. The metastable state (a^5S_2) atom, in contrast, favors a surface location, which is suggested by DFT calculations (Ref.[45]) and is supported by the experimental observations, as follows.

We start with the a^5S_2 atom, because the in-droplet $A^1\Sigma_u^+ \leftarrow X^1\Sigma_g^+$ molecule band overlaps in energy with the atom $y^5P_{1,2,3}^\circ \leftarrow a^5S_2$ transition, leading to excited Cr* (y^5P°) atoms which are photoionized by absorption of two photons (Fig. 1), so that Cr$^+$ ions are detected upon detachment from the droplet. In the Cr$^+$ signal in Fig. 2 (a), all three peaks of the $y^5P_{1,2,3}^\circ \leftarrow a^5S_2$ transition are observable. Considering the detailed Cr$^+$ scan (Fig. 3) of the most intense $y^5P_3^\circ \leftarrow a^5S_2$ peak, the onset of the main feature is shifted approximately 5 cm^{-1} to the blue relative to the bare atom transition energy. A maximum is reached at 22240 cm^{-1} followed by an almost steady signal decrease, giving a total peak width of $\sim$50 cm^{-1}. These spectral characteristics are comparable to transitions of heavier alkali metal atoms that reside in a surface dimple[27,35,46], which is a first indication for the surface location of the a^5S_2 atom (furthers to follow). At the bare atom transition energy (indicated with a vertical line in the detailed scan in Fig. 3), the absence of sharp atomic lines proves that

hardly any atoms are ejected from the droplet upon dissociation, encouraging the interpretation in terms of the effective kinetic energy dissipation upon predissociation.

We consider it important to mention that the Cr $y^5P_{1,2,3}^\circ \leftarrow a^5S_2$ excitation observed here on the He_N surface is of completely different nature than the $z^5P^\circ \leftarrow a^5S_2$ excitation of bare Cr atoms and small Cr-He$_n$ ($n = 1, 2, ...$) exciplexes observed in our previous studies[23]. This becomes obvious by comparing the corresponding line shapes. In the two-color REMPI scheme in Ref.[23], 308 nm excitation and droplet mediated relaxation results in bare a^5S_2 Cr atoms and Cr-He$_n$ exciplexes, both being ejected from the He_N. The corresponding excitation spectrum is composed of a sharp atom line accompanied by a wing to the blue (due to Cr-He$_n$). Here, in contrast, we find hardly any signal at the bare atom line position (Fig. 3) and observe the onset of the peak 5 cm^{-1} to the blue. Although the XeCl laser was present for recording the spectra in Fig. 3, a bare atom transition peak is hardly detectable. Systematic studies showed an increased bare atom signal for higher XeCl laser fluence, which starts causing the ejection process.

We now turn to the location and environment of the other dissociation fragment - the a^7S ground state atom - based on the two dye laser experiment. The first laser excites the dissociating $A^1\Sigma_u^+ \leftarrow X^1\Sigma_g^+$ Cr$_2$ transition and the second laser the a^7S REMPI. Fig. 4 (a) shows the a^7S REMPI spectrum, recorded from the dissociation fragment. The fact that a^7S atoms are detected by the differential scheme proves the proposed predissociation mechanism. The spectrum is compared to the reference spectrum obtained from single atom doped He_N (black line)[21]. The spectral similarity of the broad structure, which represents the in-droplet broadened $y^7P_{2,3,4}^\circ \leftarrow a^7S_3$ transition, indicates a well defined separation after dissociation of the ground state atom from the a^5S_2 atom on the surface. If both dissociation fragments resided inside the He_N, one would expect a spectral line shift like it was observed for Mg atoms ($\frac{\Delta\bar{\nu}}{\bar{\nu}} \sim 2$ %)[47]. Hence, the spectral similarity of a^7S_3 atoms from dissociated Cr$_2$ and original a^7S_3 atoms is a further indication of the interior location of the ground state fragment and the surface location of the a^5S_2 atom fragment.

To show the stable position of both fragments after dissociation, the probe laser was time-delayed ($\Delta\tau \sim 20$ ns) to avoid a temporal overlap between the dissociation pump laser and the ionizing probe laser pulse. The pump-probe delay has no significant influence on the spectrum. Hence, no indication for a recombination or spatial approach between both neutral fragments within the delay time is found. We thus conclude that the Cr a^5S_2 atom is stable on the He_N surface, where it is available for further excitation.

It is important to point out that despite the attractive interaction between the center-located ground state and the surface-

located metastable state atoms, molecule formation does not occur. This indicates an energy barrier between the two atoms as a result of the confining potential energy curve of the solvated atom and the attractive Cr_2 (a^7S_3-a^5S_2) potential energy curve, in a similar way as it was recently calculated for the Rb-Xe van der Waals system in a He_{500} droplet[27].

4.3 $Cr^+_{2,3,4}$ from Cr_2 and Small Cr_n Cluster

The characteristic atomic $y^5P^\circ_{1,2,3} \leftarrow a^5S_2$ transition peaks are also present in the REMPI spectra employing Cr^+_2 detection (see Figs. 2 (a) and 3), with exactly the same position and shape as for Cr^+ detection. This is very surprising, because the Cr atom $y^5P^\circ_{1,2,3} \leftarrow a^5S_2$ transition obviously has to be a step in the ionization process leading from Cr_2 to Cr^+_2. The observation becomes plausible when we build on the results from before, namely that upon Cr_2 dissociation the a^5S_2 atom is residing on the surface while the a^7S_3 atom remains solvated inside the droplet. After resonant ionization of the surface atom with a^5S REMPI (see Fig. 1), the Cr^+ ion has a fair chance to be pulled inside the He_N [32,34,45] where it recombines with its original partner to form Cr^+_2. Forming the Cr^+_2 $a^2\Sigma^+_g$ ground state ($Cr(^7S)+Cr^+(^6S)$, binding energy = 1.30 eV[38]), releases approximately the same amount of energy to the droplet as the initial Cr_2 formation, evaporating $\sim$2100 He atoms. A certain fraction of the droplets is now completely evaporated by this energy input which produces detectable, bare Cr^+_2 ions[9]. Remaining Cr^+_2 doped droplets that survived are not detected within the QMS mass window.

To verify Cr_2 doped He_N as the parent species of the Cr^+_2 ions, the Cr^+_2 ion yield was recorded while increasing the Cr oven temperature, and hence, the probability distribution for the formation of different Cr_n cluster sizes[36]. The Cr^+_2 ion signal shows a clear dependence on the pick-up oven temperature. For reference, the number of $Cr^+_{1,2,3,...}$ ions obtained with electron impact ionization of the doped He_N, is also recorded in dependence on the pick-up oven temperature. Keeping possible fragmentation in mind, the comparison allows an assignment of the Cr^+_2 $y^5P^\circ_3 \leftarrow a^5S_2$ signal (Fig. 2 (a), blue line, 22257 cm^{-1}) to Cr_2 doped He_N.

We mention that in addition to the $Cr+Cr^+ \rightarrow Cr^+_2$ recombination, another recombination path is possible, although unlikely. According to DFT calculations[45], $Cr^\star$ y^5P° atoms have a stable position on the surface and inside the He_N, with a small energy barrier in between. Hence, the $Cr^\star$ (y^5P°) atom might move back inside the droplet to form an excited $Cr^\star_2$ molecule with the Cr (a^7S_3) ground state atom. As above, evaporation of a certain fraction of the droplets and subsequent two photon ionization would lead to Cr^+_2 detection. Irrespective of the recombination path, the recombination process is restricted to the volume of the droplet. The Cr^+_2 detection after

a^5S REMPI proves the location of both dissociation fragments to be on the droplet.

Now we consider He_N doped with $Cr_{3,4}$ clusters. Fig. 3 shows that at the Cr atom $y^5P^\circ_3 \leftarrow a^5S_2$ transition also Cr^+_3 and Cr^+_4 ion clusters are detected. This means, He_N doped with Cr_3 and Cr_4 (probably also Cr_5,...) clusters can undergo a similar excitation process as Cr_2, including the characteristic a^5S REMPI of a surface located atom and subsequent recombination with the solvated fragments. Because of the strong Cr_2 bonding nature, Cr_3 is composed of a dimer plus a loosely bonded atom[48,49] and Cr_4 of two dimers with strong intradimer but weak interdimer bonding[50]. This dimerization effect controls the cluster growth up to Cr_{11}, yielding similarities between the ground state photoabsorption spectra of dimers and small chromium clusters[50–52]. The detection of Cr^+_3 and Cr^+_4 therefore suggests that the Cr_2 dissociation process and surface migration of one atom is not disturbed by the presence of a further Cr atom or dimer in the droplet.

4.4 Cr_2 excitation spectrum

Now we turn to the Cr_2 $A^1\Sigma^+_u \leftarrow X^1\Sigma^+_g$ excitation band, in particular to the broad band stretching from 21500 to 22750 cm^{-1} that is present in the Cr^+ signal of the one-color REMPI scheme, shown as black curve in Fig. 2 (a). We will now show that the signal of the broad band can be assigned to Cr_2 molecules and arises from direct multiphoton ionization and subsequent dissociation to Cr and Cr^+, an ionization path that does not include Cr_2 predissociation. Outside the spectral regions of the $y^5P^\circ_{1,2,3} \leftarrow a^5S_2$ transitions, i.e., without resonance enhancement, the ionization probability of both Cr atoms resulting from dissociation is estimated to be lower than a resonant ionization via vibronic levels of the Cr_2 molecule before dissociation (see Fig. 1). Hence, we account resonant multiphoton ionization of Cr_2 in combination with efficient dissociation to Cr and Cr^+ to be responsible for the observed signal.

It is instructive to compare the band obtained with one-color REMPI (Fig. 2 (a)) to Fig. 2 (b), which shows the Cr^+ signal of the two-laser a^7S REMPI scheme where the dissociating laser is scanned. It is important to recall the following two points: (1) The a^7S REMPI is obtained from resonant ionization of the center located ground state atoms that are produced via Cr_2 predissociation. (2) The a^7S REMPI is exclusively sensitive to Cr_2 molecules and not to larger Cr_n clusters, as discussed in Section 4.2. Therefore, Fig. 2 (b) represents the Cr_2 excitation spectrum, which shows good overall agreement with the one-color REMPI band in Fig. 2 (a). The extra features in the one-color REMPI spectrum in Fig. 2 (a) with respect to the a^7S REMPI spectrum in Fig. 2 (b) indicate the presence of resonances in this ionization path. This interpretation is supported by monitoring the one-color REMPI Cr^+ yield at the spectral positions marked with asterisks in Fig. 2 (a) while increasing

the evaporation oven temperature and comparing this signal to electron bombardment ion yield, as above. It is found that at all three spectral positions the Cr^+ ion signal can be assigned predominantly to Cr_2 and not to larger Cr_n cluster.

The predissociation process, which is observed by the formation of ground state a^7S and metastable state a^5S atoms, has been reported for the $A^1\Sigma_u^+ \leftarrow X^1\Sigma_g^+$ excitation in literature [37,40,41,43]. We note that the Cr_2 might additionally be formed in higher multiplicities as it was observed for Ag_2 in He_N [53]. However, currently we cannot identify other multiplicities. For the strongly bound Cr_2 singlet ground state (binding energy = 1.42 eV $(11450\ cm^{-1})$ [38]), the majority of droplets are expected to survive the formation for a size distribution maximum of $\hat{N} = 6300$ and an energy of 5 cm^{-1} dissipated per evaporated He atom. In gas phase, the $A^1\Sigma_u^+ \leftarrow X^1\Sigma_g^+$ Cr_2 transition is observed at an energy of 21751 cm^{-1} (0-0 band, 2.7 eV) [41,43,54]. Cr_2 excitation spectra in other solid rare gas matrices yield usually shifted and broadened spectral features, but cannot provide a consistent picture about the magnitude of the shift [40,51,52,55,56].

5 Conclusions

In conclusion, we have investigated the electronic $A^1\Sigma_u^+ \leftarrow X^1\Sigma_g^+$ excitation of Cr_2 molecules located inside He_N with resonant multiphoton ionization spectroscopy, applying one- and two-laser schemes. The ionization spectra show, in addition to the droplet broadened molecular excitation structure, three pronounced peaks which we allocate to the $y^5P_{1,2,3}^\circ \leftarrow a^5S_2$ Cr atomic transitions. We conclude that the Cr_2 molecule dissociates upon excitation [41] into a solvated, ground state (a^7S_3) atom and a surface-located, metastable (a^5S_2) atom. The latter is ionized by resonance-enhanced multiphoton ionization. The conclusion is based on (a) the $y^5P_{1,2,3}^\circ \leftarrow a^5S_2$ transition line shape (50 cm^{-1} width and a 5 cm^{-1} blueshift of the onset with respect to the bare atom lines), (b) a two laser experiment with REMPI detection of the produced a^7S_3 atoms, and (c) theoretical simulations of the a^5S_2 atom location [45]. Surprisingly, we detect these three $y^5P_{1,2,3}^\circ \leftarrow a^5S_2$ atom peaks not only at the Cr^+ ion mass, but also at $Cr_{2,3,4}^+$ masses. Cr_2^+ detection demonstrates that upon photoionization, a fraction of the surface atoms migrates back inside the droplet to recombine with their ground state counterpart. The $Cr_{3,4}^+$ detection indicates that this pairwise dissociation and surface migration process is not disturbed by the presence of additional Cr atoms, a fact which we attribute to the strong dimerization effect in small Cr clusters [50].

The elucidated mechanisms open a possibility for photoinduced chemistry mediated by He_N. Chemical reactions in He_N doped with both surface located (e.g., alkali-metal or alkaline earth metal atoms) and solvated species could be triggered by

photoexcitation of the latter to a surface located state. The bond formation can then be followed, e.g., with time-resolved femtosecond spectroscopy.

6 Acknowledgement

References

1 C. Callegari and W. E. Ernst, *Helium Droplets as Nanocryostats for Molecular Spectroscopy - from the Vacuum Ultraviolet to the Microwave Regime. - in: Handbook of High-Resolution Spectroscopy*, John Wiley & Sons, Chinchester, 2011.

2 J. M. Merritt, J. Kupper and R. E. Miller, *Phys. Chem. Chem. Phys.*, 2005, **7**, 67 – 78.

3 J. M. Merritt, S. Rudić and R. E. Miller, *J. Chem. Phys.*, 2006, **124**, 084301–1 – 084301–12.

4 S. Rudić, J. M. Merritt and R. E. Miller, *J. Chem. Phys.*, 2006, **124**, 104305–1 – 104305–8.

5 J. Küpper and J. M. Merritt, *Int. Rev. Phys. Chem.*, 2007, **26**, 249 – 287.

6 A. M. Morrison, J. Agarwal, H. F. Schaefer and G. E. Douberly, *J. Phys. Chem. A*, 2012, **116**, 5299–5304.

7 K. von Haeften, A. Metzelthin, S. Rudolph, V. Staemmler and M. Havenith, *Phys. Rev. Lett.*, 2005, **95**, 215301–1 – 215301–4.

8 D. Stolyarov, E. Polyakova and C. Wittig, *J. Phys. Chem. A*, 2004, **108**, 9841 – 9846.

9 A. Braun and M. Drabbels, *J. Chem. Phys.*, 2007, **127**, 114305–1 – 114305–6.

10 K. Nauta and R. E. Miller, *Science*, 1999, **283**, 1895 – 1897.

11 K. Nauta and R. E. Miller, *Science*, 2000, **287**, 293 – 295.

12 G. E. Douberly and R. E. Miller, *J. Phys. Chem. A*, 2007, **111**, 7292 – 7302.

13 G. E. Douberly, J. M. Merritt and R. E. Miller, *Phys. Chem. Chem. Phys.*, 2005, **7**, 463 – 468.

14 T. Liang, S. D. Flynn, A. M. Morrison and G. E. Douberly, *J. Phys. Chem. A*, 2011, **115**, 7437 – 7447.

15 F. Ancilotto, P. B. Lerner and M. W. Cole, *J. Low Temp. Phys.*, 1995, **101**, 1123 – 1146.

16 F. Federmann, K. Hoffmann, N. Quaas and J. D. Close, *Phys. Rev. Lett.*, 1999, **83**, 2548 – 2551.

17 N. B. Brauer, S. Smolarek, E. Loginov, D. Mateo, A. Hernando, M. Pi, M. Barranco, W. J. Buma and M. Drabbels, *Phys. Rev. Lett.*, 2013, **111**, 153002–1 – 153002–6.

18 D. Mateo, A. Hernando, M. Barranco, E. Loginov, M. Drabbels and M. Pi, *Phys. Chem. Chem. Phys.*, 2013, **15**, 18388 – 18400.

19 F. Lindebner, A. Kautsch, M. Koch and W. E. Ernst, *Int. J. Mass Spectrom.*, 2014, **365-366**, 255 – 259.

20 F. Cargnoni and M. Mella, *J. Phys. Chem. A*, 2011, **115**, 7141 – 7152.

21 A. Kautsch, M. Hasewend, M. Koch and W. E. Ernst, *Phys. Rev. A*, 2012, **86**, 033428–1 – 033428–4.

22 A. Kautsch, M. Koch and W. E. Ernst, *J. Phys. Chem. A*, 2013, **117**, 9621 – 9625.

23 M. Koch, A. Kautsch, F. Lackner and W. E. Ernst, *J. Phys. Chem. A*, 2014, **118**, 8373 – 8379.

24 A. Braun and M. Drabbels, *Phys. Rev. Lett.*, 2004, **93**, 253401–1 – 253401–4.

25 A. Braun and M. Drabbels, *J. Chem. Phys.*, 2007, **127**, 114303–1 – 114303–14.

26 E. Polyakova, D. Stolyarov and C. Wittig, *J. Chem. Phys.*, 2006, **124**, 214308–1 – 214308–11.

27 J. Poms, A. W. Hauser and W. E. Ernst, *Phys. Chem. Chem. Phys.*, 2012, **14**, 15158 – 15165.

28 A. Masson, M. Briant, A. Hernando, N. Halberstadt, J.-M. Mestdagh and M.-A. Gaveau, *J. Chem. Phys.*, 2012, **137**, 184310–1 – 184310–9.

29 E. Lugovoj, J. P. Toennies and A. Vilesov, *J. Chem. Phys.*, 2000, **112**, 8217 – 8220.

30 G. E. Douberly, P. L. Stiles, R. E. Miller, R. Schmied and K. K. Lehmann, *J. Phys. Chem. A*, 2010, **114**, 3391 – 3402.

31 L. An der Lan, P. Bartl, C. Leidlmair, R. Jochum, S. Denifl, O. Echt and P. Scheier, *Chem. Eur. J.*, 2012, **18**, 4411 – 4418.

32 M. Theisen, F. Lackner and W. E. Ernst, *Phys. Chem. Chem. Phys.*, 2010, **12**, 14861 – 14863.

33 M. Theisen, F. Lackner, G. Krois and W. E. Ernst, *J. Phys. Chem. Lett.*, 2011, **2**, 2778 – 2782.

34 X. Zhang and M. Drabbels, *J. Chem. Phys.*, 2012, **137**, 051102–1 – 051102–4.

35 M. Koch, J. Lanzersdorfer, C. Callegari, J. S. Muenter and W. E. Ernst, *J. Phys. Chem. A*, 2009, **113**, 13347 – 13356.

36 M. Ratschek, M. Koch and W. E. Ernst, *J. Chem. Phys.*, 2012, **136**, 104201–1 – 104201–6.

37 K. Andersson, *Chem. Phys. Lett.*, 1995, **237**, 212 – 221.

38 C.-X. Su, D. A. Hales and P. Armentrout, *Chem. Phys. Lett.*, 1993, **201**, 199 – 204.

39 A. Kramida, Yu. Ralchenko, J. Reader and NIST ASD Team (2012). NIST Atomic Spectra Database (ver. 5.0), [Online]. Available: http://physics.nist.gov/asd [2013, May 16]. National Institute of Standards and Technology, Gaithersburg, MD.

40 M. J. Pellin and D. M. Gruen, *J. Chem. Phys.*, 1983, **79**, 5887 – 5893.

41 S. J. Riley, E. K. Parks, L. G. Pobo and S. Wexler, *J. Chem. Phys.*, 1983, **79**, 2577 – 2582.

42 J. Higgins, C. Callegari, J. Reho, F. Stienkemeier, W. E. Ernst, K. K. Lehmann, M. Gutowski and G. Scoles, *Science*, 1996, **273**, 629 – 631.

43 V. Bondybey and J. English, *Chem. Phys. Lett.*, 1983, **94**, 443 – 447.

44 J. V. Pototschnig, M. Ratschek, A. W. Hauser and W. E. Ernst, *Phys. Chem. Chem. Phys.*, 2014, **16**, 9469 – 9478.

45 M. Ratschek, J. V. Pototschnig, A. W. Hauser and W. E. Ernst, *J. Phys. Chem. A*, 2014, **118**, 6622 – 6631.

46 G. Auböck, J. Nagl, C. Callegari and W. E. Ernst, *Phys. Rev. Lett.*, 2008, **101**, 035301–1 – 035301–4.

47 A. Przystawik, S. Göde, T. Döppner, J. Tiggesbäumker and K.-H. Meiwes-Broer, *Phys. Rev. A*, 2008, **78**, 021202–1 – 021202–4.

48 H. Cheng and L.-S. Wang, *Phys. Rev. Lett.*, 1996, **77**, 51 – 54.

49 L.-S. Wang, H. Wu and H. Cheng, *Phys. Rev. B*, 1997, **55**, 12884 – 12887.

50 J. I. Martínez and J. A. Alonso, *Phys. Rev. B*, 2007, **76**, 205409–1 – 205409–5.

51 L. Fang, B. Davis, H. Lu and J. R. Lombardi, *J. Phys. Chem. A*, 2001, **105**, 9375 – 9378.

52 J. Derouault and M. Dalibart, *Z. Phys. D: At. Mol. Clusters*, 1991, **19**, 211 – 214.

53 A. Przystawik, P. Radcliffe, S. Göde, K. H. Meiwes-Broer and J. Tiggesbäumker, *J. Phys. B: At. Mol. Opt. Phys.*, 2006, **39**, S1183 – S1189.

54 D. L. Michalopoulos, M. E. Geusic, S. G. Hansen, D. E. Powers and R. E. Smalley, *J. Phys. Chem.*, 1982, **86**, 3914 – 3916.

55 E. P. Kündig, M. Moskovits and G. A. Ozin, *Nature*, 1975, **254**, 503 – 504.

56 M. Vala, R. Pyzalski, J. Shakhsemampour, M. Eyring, J. Pyka, T. Tipton and J. C. Rivoal, *J. Chem. Phys.*, 1987, **86**, 5951 – 5957.